Journal of Marine Research, 59, 895–919, 2001

Central equatorial Pacific zonal currents. I: The Sverdrup balance, nonlinearity and tropical instability waves. Annual mean dynamics

by D. E. Harrison[1,2], R. D. Romea[1] and S. H. Hankin[1]

ABSTRACT

Several recent observational studies of central Pacific equatorial current dynamics have suggested that, in the vertical integral between the surface and the thermocline, the linear equatorial Sverdrup balance holds. However, in a high vertical resolution ocean general circulation model, we find that nonlinearity is an order (1) element of the local and the vertically integrated balances on and near the equator at 140W. Although this OGCM has been used in many studies of the tropical Pacific, its equatorial zonal momentum equation balances have never been described in detail and compared with observations. We describe the annual mean balances here, identify the similarities and differences between the model balances and observational estimates of the balances, and discuss various reasons why the model and the observations may disagree in the respects that they are found to do so.

The term balances vary strongly with latitude and depth; the system is nonlinear and three dimensional. There is little tendency for pairs of terms (e.g., the meridional and vertical advection terms) to balance locally or in the vertical integral. Every term in the zonal momentum equation plays a role somewhere in the analysis region discussed here. Thus the generality of point estimates of these balances is small. The Tropical Instability Wave zonal momentum flux divergence, although not an $O(1)$ term in the balance, acts like a 'negative viscosity' over the upper 40 m on the equator; its tendency is to drive westward flow. If the ocean balances resemble those of the model dynamics, gaining detailed perspective on the zonal balances will require a major observational effort. Because there is strong subseasonal and interannual variability of the flows in the central equatorial Pacific, time-mean balances are not simple to estimate. Further, special attention will have to be given to resolving the shears in the upper 50 m, because it is over these depths that the model and observational results differ most strongly. We suggest that the widely used technique of extrapolating the near-surface currents based on their shears in the uppermost bins of the ADCP profiles deserves careful scrutiny; subsampling the model flow profiles in this fashion leads to important errors. Until the strong vertically sheared very near-surface current field is observed accurately it will not be possible to determine if the model results are correct, but we suggest that the existing observational results should not be regarded as definitive.

1. PMEL/NOAA, 7600 Sand Point Way, NE, Seattle, Washington, 98115, U.S.A. ***email: harrison@pmel.noaa.gov***

2. Joint Institute for the Study of the Atmosphere and Ocean (JISAO), University of Washington, Box 354235, Seattle, Washington, 98195, U.S.A.

1. Introduction

The classical linear equilibrium theory of the Equatorial Undercurrent (EUC), the "Equatorial Sverdrup balance," postulates a vertically integrated (between the surface and thermocline) balance between the zonal wind stress (westward) and the zonal pressure gradient (eastward). In the classical two-dimensional vertical circulation, there is wind-forced Ekman poleward surface flow, which creates a surface divergence that is balanced by equatorward inflow in the thermocline and upwelling in the Equatorial Undercurrent (EUC). Vorticity conservation implies that this meridional circulation will typically be nonlinear in its local balances, for wind stress values typical of the central tropical Pacific, but the vertically integrated balance can still be linear in principle.

Several recent papers (Yu and McPhaden, 1999a, henceforth YM; Qiao and Weisberg, 1997, henceforth QW; Johnson and Luther, 1994, henceforth JL) have estimated the long-time mean zonal momentum balances of the upper equatorial Pacific Ocean from different data sets. These papers present results that support the linear equilibrium theory. The YM and QW studies are based in part on long time series of observed near-equatorial currents, made with subsurface upward-looking acoustic Doppler profiling current meter (ADCP) moorings between 165E and 95W (see McPhaden and Hayes, 1990; Yu and McPhaden, 1999b and QW for details of the observations). As the QW study (the only one designed to address the zonal momentum balance) was centered at 140W, we present the model balances along this longitude.

YM based their dynamical analysis on a multi-year series of observed near-equatorial currents, made with 5 ADCP moorings between 165E and 90W along the equator. Time series of six years or longer, ending by May of 1997, were used. This Tropical Atmosphere-Ocean (TAO) buoy array was implemented as part of the Tropical Ocean Global Atmosphere (TOGA) program. At 140W, and for some of the time, the ADCPs were supplemented by mechanical current meters (MCM), which measured currents at 10 m depth. They report that ADCP zonal velocity, extrapolated from 30–40 m to 10 m, is well correlated with the MCM. The ADCP data are extrapolated to the sea surface. Zonal advection is estimated by finite-differencing the data. Their dataset does not allow estimates of the meridional or vertical advective terms. They claim, appealing in part to QW, that these terms tend to cancel each other, and conclude that, in the mean, the balance is mainly between zonal wind stress and depth-integrated zonal pressure gradient, in good agreement with linear Sverdrup theory. The model balances presented here do not support the idea that the meridional and vertical advective terms cancel closely enough to permit them to be neglected.

JL estimated the mean zonal momentum balance in the upper and central equatorial Pacific Ocean near 160W, using roughly monthly-sampled ADCP velocities and conductivity-temperature-depth (CTD) measurements from the North Pacific Experiment (NORPAX) Hawaii-to-Tahiti Shuttle Experiment, which were taken between February 1979 and June 1980. They claim that the ADCP instruments returned reliable velocities from depths between 26 and 117 m, in 6.5 m bins (every second bin is independent).

Estimated errors in their computed vertical velocity field are large (order of the velocity itself), and the structure of mean vertical velocity is only poorly distinguished from zero. In addition, they averaged mean vertical velocity over 3° of latitude, in order to reduce errors. Their estimated mean quantities have uncertainties from the lack of time resolution to sample the Tropical Instability Waves (TIWs), and because the time duration was only 18 months of an ocean that exhibits strong variability on subseasonal as well as interannual time scales. However, we shall see that in the thermocline, the model balances resemble the balances estimated by JL in many respects.

QW made estimates of the zonal momentum balance in and above the EUC using data taken from five ADCP moorings deployed in a diamond-shaped array about (140W, 0N) from 12 May 1990 to 18 June 1991, as part of the TOGA Tropical Instability Wave Experiment (TIWE). The three equatorial moorings were at 142W, 140W, and 138W, and the two off-equatorial moorings were located at 140W and 1S and 1N. ADCP measurements were obtained up to 30 m, and the velocity field between 30 m and the surface was estimated by linear extrapolation using the 30–40 m shear. The array was designed to provide a three-dimensional view of the circulation, where vertical velocity $w(z)$ was obtained by vertically integrating the continuity equation between the surface and depth z. The horizontal derivatives were computed with central differences, so that $\Delta x = 4°$ (longitude) and $\Delta y = 2°$ (latitude). This study had excellent time resolution but sampled only a one-year period and had to rely on very simple differences to estimate both the equatorial vertical velocity profile and the advective terms.

The primitive equation tropical ocean general circulation model used here was first used by Philander and colleagues in the late 1970s. It has been used to investigate many aspects of tropical ocean variability, both in 'process' mode and simulation mode, and has reproduced many aspects of the observed circulations and their variability (e.g. Philander *et al.,* 1987; Stockdale *et al.,* 1998). Despite the wide range of studies that have been carried out with it, the detailed zonal momentum equation balances that hold when it well simulated the near-equatorial circulation have not been described in detail. We here report the annual mean balances, at 140W, of such a study and find that, while there are similarities with the balances estimated in the thermocline, the model balances near the surface are much more strongly nonlinear. In part, this results from the strength of the near-surface model vertical velocity field, but also from differences in the profile of the meridional flow. The model near-surface nonlinearity is sufficient that the vertically integrated zonal momentum balance is not Sverdrup to lowest order.

The model experiment results described here represent the annual mean of a climatological seasonal cycle experiment that successfully simulates a wide range of observations. It has a seasonal cycle of SST, equatorial zonal currents and tropical instability waves (TIWs) that have amplitudes and cycles very much like the reported fields, as we shall show. In this paper we shall present only the annual mean flow, variances and covariances (when data are available for comparison) near 140W; in the companion paper (Harrison *et al.,* 2001) we present the seasonal cycle, comparison with observations, and discuss the dynamics of

this cycle. Within the computational framework of the model, we can evaluate all the terms in the zonal momentum balance. Wacongne (1989, 1990) presented aspects of the zonal momentum balance in the central equatorial Atlantic and Pacific, but the present Pacific simulation is more realistic and the balances presented here are comprehensive. We shall show that there are some significant agreements between the model balances and the published observational estimates, but also important differences, particularly in the vertically integrated balances. We shall argue below that, where there are inconsistencies between our model and the reported observational mean zonal momentum balances, limitations of the observations and the approximations used to estimate the terms in the zonal momentum balance from them may explain a significant amount of the differences.

There is significant zonal variation of the current fields and the zonal momentum balances along the equator. The thermocline and the core of the Equatorial Undercurrent shallow as one moves farther east, and the vertical profile of the zonal pressure gradient changes significantly also. In the interest of brevity we only present results here for 140W, a location at which many observations are available and where two of the three observational studies were done. Particularly east of 110W, when the EUC is decelerating strongly, the zonal momentum balances are quite different than those described here, but there are differences at 165W and 125W as well. Future field work in the eastern equatorial Pacific is being planned, and model-observation comparisons will likely be appropriate in this region in coming years.

In Section 2 we describe briefly the model and the details of the experiment. The near-equatorial annual mean circulation is presented in Section 3, and its local zonal momentum equation balances are described in Section 4. The vertically integrated zonal momentum balances, from the surface downward through the thermocline, are given in Section 5. The statistics of the model TIWs are described in Section 6 and compared with observations. We discuss these results, and provide further comparison with the observational results in Section 7. In particular, we present a simulation of the ADCP sampling of the numerical model results, suggesting that it may be the inability of the instruments used in the YM, QW and JL observational studies to resolve this near-surface flow, and to accurately compute horizontal derivatives (and by extension the vertical velocity) that lead to their conclusion.

2. Description of the model

The model results described in this study were obtained by constructing the annual average over the last year of a seasonal cycle experiment using a version of the GFDL primitive-equation ocean circulation model of the tropical Pacific Ocean as discussed in detail by Philander and Seigel (1985), Philander *et al.* (1987) and Harrison *et al.* (1989) and their references. This model system was developed by Philander and Pacanowski in the 1980s and we have tuned it further against observations. The coastlines and gridpoint distribution are shown in Figure 2 of Philander *et al.* (1987). The model domain extends from 30S to 50N, and from 140E to 80W. There is a constant 1° zonal grid separation and

varying meridional grid separation ($\frac{1}{3}°$ resolution within 10° of the equator). As used here, the model has a flat-bottom (4000 m deep), with 27 levels in the vertical (the upper grid point is at 5 m, with 10 m grid separation over the upper 100 m and increasing below that). The horizontal mixing equatorward of 10° latitude is by eddy viscosity ($A_{mH} = 10^7$ cm^2/s) and eddy heat diffusion ($A_{hH} = 2 \times 10^7$ cm^2/s). Poleward of this, these values increase gradually. This value of A_{mH} is one-half that used by Philander and Seigel (1985; seasonal cycle in the tropical Pacific Ocean) and Wacongne (1989; equatorial Atlantic Ocean) but the same as Wacongne (1990), who discusses some elements of the annual mean dynamics of the Pacific undercurrent. Relative to the Philander and Seigel (1985) seasonal cycle results, our lower value improves the correspondence of the model flows with observations. Vertical mixing is done by the Pacanowski and Philander (1981) version of Richardson-number (Ri) dependent mixing and early Cox-style convective adjustment to remove vertical instability. At the surface, a minimum value of the vertical diffusion coefficient ($A_{mV} = 10$ cm^2/s) is chosen to simulate wind stirring by scales not resolved by the model. For regions where $Ri \leq \frac{1}{4}$, a value of $A_{mV} = 50$ cm^2/s is chosen to simulate vertical instability. Calculation of the annual mean profile for A_{mV}, derived from the model vertical mixing parameterization, shows values on the equator of about 50 cm^2/s near the surface dropping smoothly to about 1 cm^2/s near the EUC core. This is consistent with estimates from data (see Fig. 19 from JL, and Fig. 14 from QW).

The model was initialized from no motion and with the temperature and salinity climatological fields in January (Levitus, 1982). The model was forced for 15 years by climatological monthly mean surface wind stresses, developed from the COADS[3] marine data set and the Large and Pond (1981) stability dependent drag coefficient (Harrison, 1989), and by the Philander and Seigel (1985) surface heat flux parameterization as modified by Harrison (1991). The model exhibits a quasi-equilibrium upper ocean seasonal current cycle by the end of the integration.

We make no claim that the present experimental results are definitive; much remains unknown about how best to model the mixing of heat, salt and momentum in models like this, about the surface forcing that drives the tropical Pacific Ocean, and about the climatological mean ocean circulation itself. But, at present the model is able to reproduce, semi-quantitatively, every reported large-scale observational feature of the central equatorial Pacific. As more data are collected, the model results will undoubtedly reveal shortcomings that will require additional simulation effort.

3. Annual mean circulation

The annual mean is the average over the last year of the integration, e.g., for zonal velocity u:

3. Comprehensive Ocean-Atmosphere Data Set, compiled from ship records over the global ocean (Woodruff *et al.,* 1987).

$$U = \frac{1}{T}\int_{t}^{t+T} u\,dt, \tag{1}$$

where t is time and T = one year. Henceforth, capitalized variables will denote the annual means. We shall denote fluctuations about the annual mean, which represent contributions from the seasonal variability, tropical instability waves and other high frequency components as primed variables, i.e.,

$$u = U + u'. \tag{2}$$

Figure 1 shows the annual mean zonal (U, positive eastward), meridional (V; positive northward) and vertical (W; positive upward) velocity fields between the surface and 250 m depth, at 140W and between 4S and 4N. Figure 2 shows profiles of the same annual mean velocities as a function of depth, at (140W, 0N), with the envelope defined by $\pm$ one standard deviation also shown; there is considerable variability from the seasonal cycle and from tropical instability waves, even in a climatology experiment like this one. These annual mean model flow patterns are quite like those computed seasonally from the Hawaii-Tahiti Shuttle data (Fig. 3 from LJ) and agree well with the record-length means from QW (their Fig. 6). In particular, the zonal flow reveals: (1) a maximum EUC speed of about 110 cm/s, (2) the EUC is confined between 2N and 2S, (3) the South Equatorial Current (SEC) is present from 4S to 4N, (4) the equatorial surface flow is westward at about 30 cm/s and (5) there is very strong near-surface vertical shear. The computed longitudinal structure of the annual mean fields at the equator (not shown) agrees well with the Tropical Atmosphere Ocean (TAO) observations (see Fig. 2 of Yu and McPhaden, 1999b). The core of the eastward EUC slopes upward to the east, with maximum flow around (140W, 0N) at around 120 m depth. Maximum speeds (100 cm/s) agree well, although the depth of the EUC maximum is about 20 m shallower in the model.

The annual mean model meridional flow shows a wind-forced cell with poleward flow near the surface (Ekman transport is confined to depths less than 35 m) and much weaker equatorward flow below this. The cell is noticeably asymmetric (which is seen even more strongly farther west at 160W by JL), with much stronger circulation in the northern hemisphere. Because the climatological zonal wind stress is stronger in the northern hemisphere, asymmetry in the Ekman flow is expected. The wind-induced meridional velocity cell exists mainly above the core of the EUC.

The mean vertical velocity field shows maximum upwelling just south of the equator at about 40 m depth (above the EUC core), and upwelling present across the meridional extent of the EUC. There is significant downwelling poleward of about 3°. The upwelling pattern is meridionally asymmetric, with upwelling extending farther into the northern hemisphere than into the southern. JL's estimate of the vertical velocity field is also strongly asymmetric, but has large uncertainty associated with it. The processes responsible for the deeper upwelling pattern are not obvious; presumably they are associated with

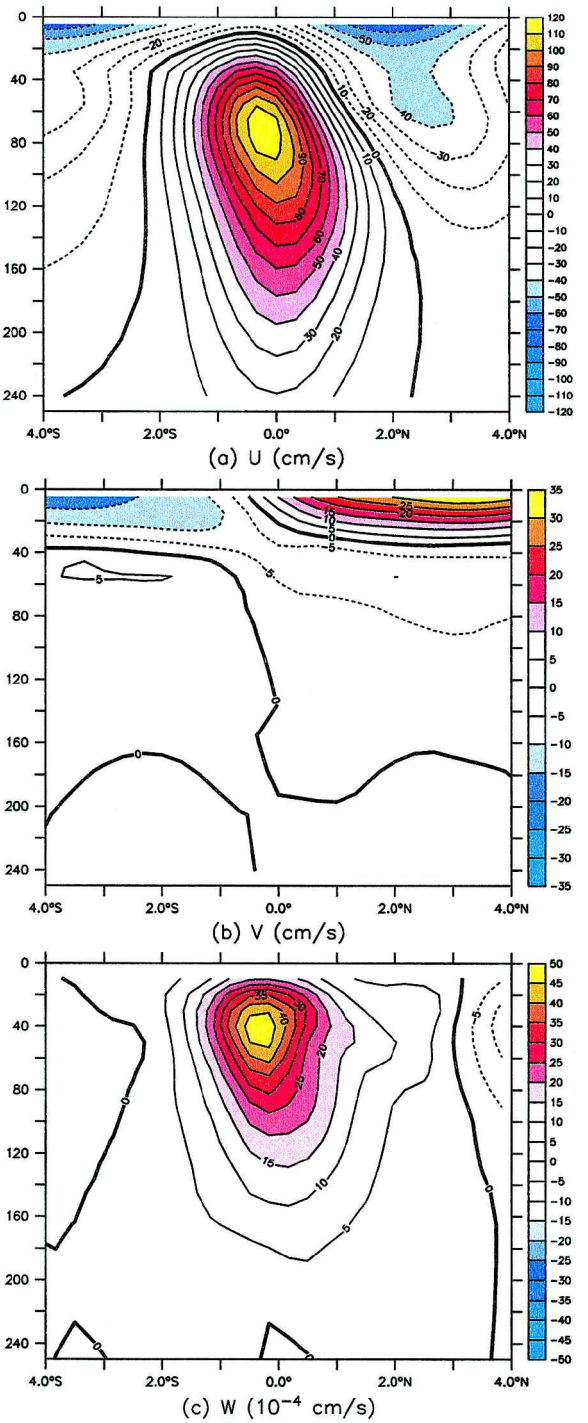

Figure 1. Model annual mean flow fields from 4S to 4N (abscissa) and over a depth range 0–250 m (ordinate) at 140W, averaged over one year of the climatological simulation (a) zonal velocity (U; cm/s; positive eastward), (b) meridional velocity (V; cm/s; positive northward), (c) vertical velocity (W; 10^{-4} cm/s; positive vertically upward). Note that, in order to elucidate the structure, each panel has a different set of contour intervals.

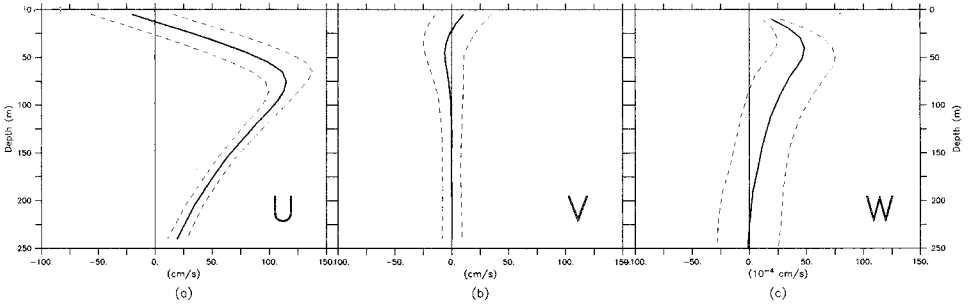

Figure 2. Model annual mean velocities, at (140W, 0N), as a function of depth; (a) zonal velocity (U; cm/s), (b) meridional velocity (V; cm/s), (c) vertical velocity (W; 10^{-4} cm/s). Also shown in each case is the envelope (dashed lines) defined by ± one standard deviation.

changes in the zonal mass transport of the EUC and waveguide-extra waveguide processes. Harrison (1996) has discussed in considerable detail the features of the vertical velocity variability in space and time in this model, using a variety of experiments.

4. The annual zonal momentum balances

We next explore the balances that control the zonal velocity by examining the terms in the zonal momentum equation:

$$\frac{\partial u}{\partial t} = -\left(u\frac{\partial u}{\partial x} + v\frac{\partial u}{\partial y} + w\frac{\partial u}{\partial z}\right) - \frac{1}{\rho}\frac{\partial p}{\partial x} + fv + A_{mH}\left(\frac{\partial^2 u}{\partial x^2} + \frac{\partial^2 v}{\partial y^2}\right) + \frac{\partial}{\partial z}\left(A_{mV}\frac{\partial u}{\partial z}\right) + \frac{\partial}{\partial z}\left(\frac{\tau^x}{\rho}\right)\delta_{i1}, \tag{3}$$

where ρ is density, p is pressure, f is the Coriolis parameter, and the horizontal and vertical eddy viscosities are represented as A_{mH} and A_{mV}, respectively. The grid is such that (u, x) is positive eastward, (v, y) is positive northward, and (w, z) is positive vertically upward. Eq. (3) is arranged such that the terms on the right-hand side represent 'tendency' terms that drive the local acceleration $(\partial u/\partial t)$ term. The last term on the right-hand side of (3) represents the contribution to the vertical mixing tendency of the zonal wind stress τ^x in the first vertical level ($i = 1$) of the model ($\delta_{i1} = 0$ if $i \neq 1$, $\delta_{i1} = 1$ if $i = 1$). Note that the term balances reported here are computed on the MOM spherical co-ordinate model grid (see e.g., Pacanowski, 1995), so that (3) is not strictly correct. However, the notation will suffice for our discussion.

We form the annual mean momentum equation by using (2) and taking a long time average of (3), term by term, assuming that $\partial U/\partial t = 0$. Because of the presence of both the seasonal variability and the TIWs, the annual mean nonlinear advective terms (the total zonal momentum tendency due to advection of zonal momentum) include both the tendency from the mean advection by the mean flow (denoted by NLA) and from the

Reynolds Stress divergence (denoted by EDDY; although no dynamical interpretation should be inferred by this name):

$$-\langle Du/Dt\rangle = -\left\langle u\frac{\partial u}{\partial x} + v\frac{\partial u}{\partial y} + w\frac{\partial u}{\partial z}\right\rangle = \text{NLA} + \text{EDDY}, \tag{4}$$

where the brackets denote an annual average, and where

$$\text{NLA} = -\left[U\frac{\partial U}{\partial x} + V\frac{\partial U}{\partial y} + W\frac{\partial U}{\partial z}\right], \tag{5a}$$

$$\text{EDDY} = -\left[\frac{\partial}{\partial x}\langle u'u'\rangle + \frac{\partial}{\partial y}\langle u'v'\rangle + \frac{\partial}{\partial z}\langle u'w'\rangle\right]. \tag{5b}$$

We shall also find it convenient to discuss the diffusion terms in (3) according to the following groupings: D_H = annual mean horizontal momentum mixing tendency, and D_Z = annual mean vertical momentum mixing tendency, i.e.,

$$D_H = A_{mH}\left(\frac{\partial^2 U}{\partial x^2} + \frac{\partial^2 V}{\partial y^2}\right), \tag{6a}$$

$$D_Z = \frac{\partial}{\partial z}\left\langle A_{mV}\frac{\partial u}{\partial z}\right\rangle + \frac{\partial}{\partial z}\left\langle\frac{\tau^x}{\rho}\right\rangle\delta_{i1}. \tag{6b}$$

Thus, the zonal momentum equation for the annual mean quantities is

$$0 = \text{NLA} + \text{EDDY} - \frac{1}{\rho}\frac{\partial P}{\partial x} + fV + D_H + D_Z. \tag{7}$$

Figure 3 shows the contributions to the annual average zonal momentum equation from the five terms in (7), at 140W and between 4S and 4N (the annual mean zonal flow is shown in the first panel for reference). Note first that the pressure gradient tendency ($-\rho^{-1}\partial P/\partial x$) does not exhibit the strong near-surface gradient that is evident in the other terms. The pressure gradient tendency is positive above 200 m, acting to accelerate the EUC eastward over almost its entire meridional and vertical extent. The tendency from the net advection of mean zonal momentum by the mean flow (NLA) also is positive (eastward) above 80 m on the equator and is strongest above 40 m between 2S and 2N, but there are cells of negative tendency (westward) just off the equator in each hemisphere between about 40 m and 100 m. The Coriolis tendency (fV) is zero on the equator, of course, but becomes positive and as large as the advective and pressure gradient tendencies by about 1.5° latitude near the surface; below 40 m fV is negative and increases rapidly poleward. The net mixing tendency ($D_H + D_Z$), which includes the effects of the zonal wind stress, is very large and negative (westward) above about 50 m between 4S and 4N, and is substantial down to about 100 m on the equator. Above 80 m, the eddy momentum flux divergence tendency (EDDY) is negative near the equator and positive from about 0.5N to 3N at the surface and from 0.5N to 4N below 40 m. As we show in Harrison and Romea (2001),

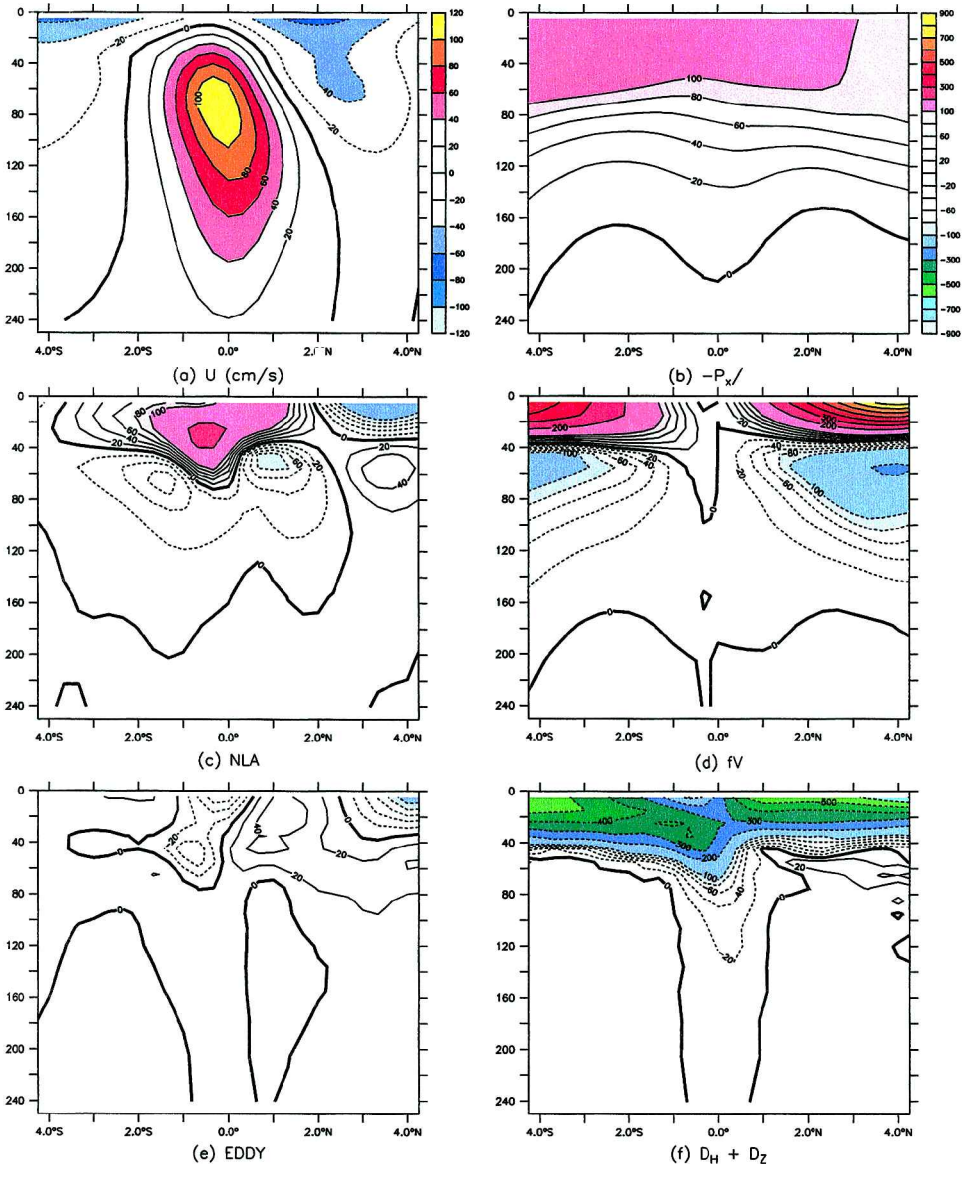

Figure 3. Annual average zonal momentum equation tendencies (see Eq. 7 and text for a discussion of the terms) at 140W and between 4S to 4N, as a function of depth. The term balances are shown in units of cm/s/month, with the convention that positive values imply an eastward tendency. (a) zonal velocity (U; cm/s) for reference, (b) zonal pressure gradient tendency ($-\rho^{-1}\partial P/\partial x$), (c) nonlinear advection of the mean zonal flow by the mean flow (NLA; see Eq. 5a in text), (d) Coriolis acceleration (fV), (e) eddy Reynolds stress divergence tendency (EDDY; see Eq. 5b in text), (f) wind forcing plus total model momentum mixing ($D = D_H + D_Z$; see Eqs. 6a and 6b in text). Contour intervals for the tendency terms are all the same (see key in panel b).

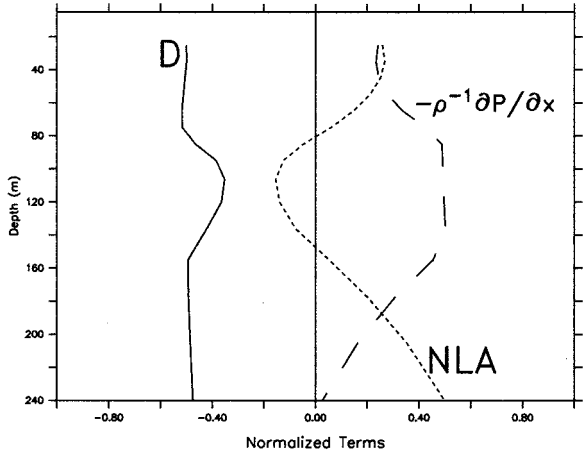

Figure 4. The relative importance of the annual mean pressure gradient tendency ($-\rho^{-1}\partial P/\partial x$), mean mixing tendency ($D = D_H + D_Z$; see Eqs. 6a and 6b in text), and the total mean nonlinear advection (NLA; see Eq. 5a in text) as a function of depth at (140W, 0N). At each vertical grid point the three terms are normalized such that the sum of their absolute values equals one.

the EDDY tendency reflects mainly the influence of tropical instability waves, which act to transfer momentum meridionally. At the surface, EDDY is about one-third the size of NLA and one-half the size of $-\rho^{-1}\partial P/\partial x$; it is relatively less important at other depths and latitudes.

The relative importance of the annual mean pressure gradient tendency ($-\rho^{-1}\partial P/\partial x$), mean mixing tendency ($D_H + D_Z$, denoted by D in the figure), and the total mean nonlinear advection tendency (denoted by NLA in the figure) as a function of depth at (140W, 0N) is shown in Figure 4. At each vertical grid point on Figure 4 the three terms are normalized such that the sum of their absolute values equals unity. All three terms are important over much of the depth range; however, the balances are different in three layers: near the surface (above the core of the EUC; 0–40 m), in the core of the EUC (40–140 m), and below the EUC (>140 m). Above 40 m, D tends to drive the flow westward, and is balanced equally by a combination of advection by the mean flow and mean zonal pressure gradient tendency. The nonlinear tendency is as strong as the pressure gradient tendency. In the EUC core depth range, the nonlinear tendency goes from westward to eastward as depth increases; below 60 m the primary eastward tendency is from the zonal pressure gradient tendency alone. At the EUC maximum, the nonlinear tendency is close to zero. Between 100 m and 180 m, nonlinearity is 30% the size of the pressure gradient tendency. Below 180 m the zonal pressure gradient tendency diminishes and the balance becomes more fully nonlinear, between eastward nonlinear acceleration tendency and westward mixing tendency.

The individual components of NLA ($-U\partial U/\partial x$, $-V\partial U/\partial y$, $-W\partial U/\partial z$) are shown in Figure 5. The individual zonal mean advection components show meridionally asymmetric cellular structures; none of the terms is symmetric about the equator. The term $-U\partial U/\partial x$

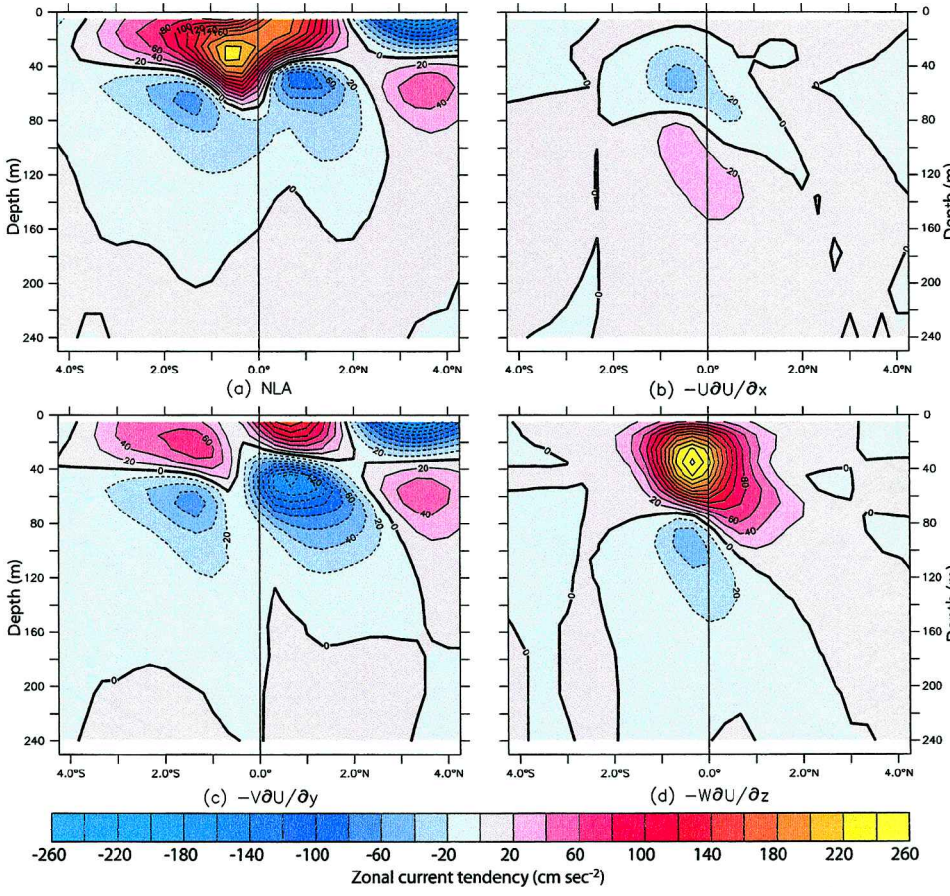

Figure 5. The individual components of the nonlinear advection of the mean zonal flow by the mean flow (NLA; see Eq. 5a in text) as a function of depth at 140W and between 4S to 4N. Contour interval = 20 cm/s/month (see key in panel b). (a) total annual mean nonlinear drive (b) $-U\partial U/\partial x$ (c) $-V\partial U/\partial y$ (d) $-W\partial u/\partial z$.

is relatively unimportant above the core of the EUC. Above the core of the EUC, and equatorward of 1°, $-W\partial U/\partial z$ dominates; however, $-V\partial U/\partial y$ is significant, particularly in the northern hemisphere. Poleward of 1°, $-V\partial U/\partial y$ dominates. Note that the QW array is unable to resolve the spatial structures of these terms, with very strong vertical gradients near the surface and horizontal gradients within 1° of the equator.

Figure 6 shows vertical profiles of the tendency terms at 140W and 2N, 1.3N, 0.7N, 0N, 0.7S and 1.35S, and illustrates the strong variations in the importance of each term both meridionally and with depth. The balances are complex and three dimensional. The picture that emerges above 40 m and between 2N and 2S is of a balance between $D_H + D_Z$ (mixing, including wind stress, denoted by D in the figures) tending to drive the flow westward, and a combination of advection by the mean flow, mean zonal pressure gradient

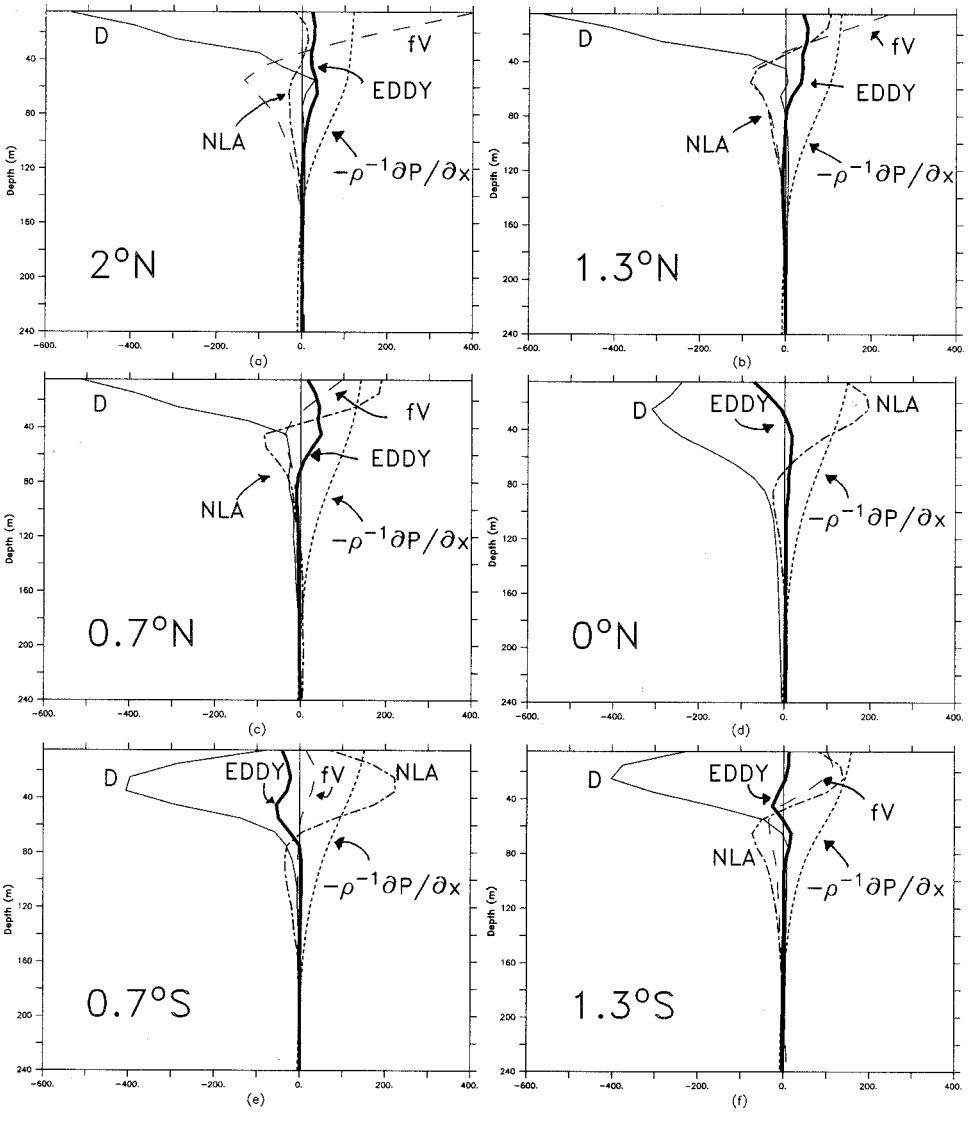

Figure 6. Vertical profiles of the annual mean zonal momentum tendency terms (see Eq. 7 and text for a discussion of the terms) at 140W plotted at various latitudes as a function of depth. Units are cm/s/month. (a) 2N, (b) 1.3N, (c) 0.7N, (d) 0N, (e) 0.7S and (f) 1.3S. NLA = nonlinear advection of the mean zonal flow by the mean flow (see Eq. 5a in text), EDDY = eddy Reynolds stress divergence tendency (see Eq. 5b in text), $D = D_H + D_Z$ = mixing tendency (wind stress and friction; see Eqs. 6a and 6b in text). Note the variations with latitude and depth of the relative importance of the terms.

tendency, and Coriolis tendency tending to drive it eastward. The EDDY tendency changes sign within this region, providing a westward tendency near and south of the equator and an eastward tendency poleward of about 0.7° latitude. Very near the equator and between

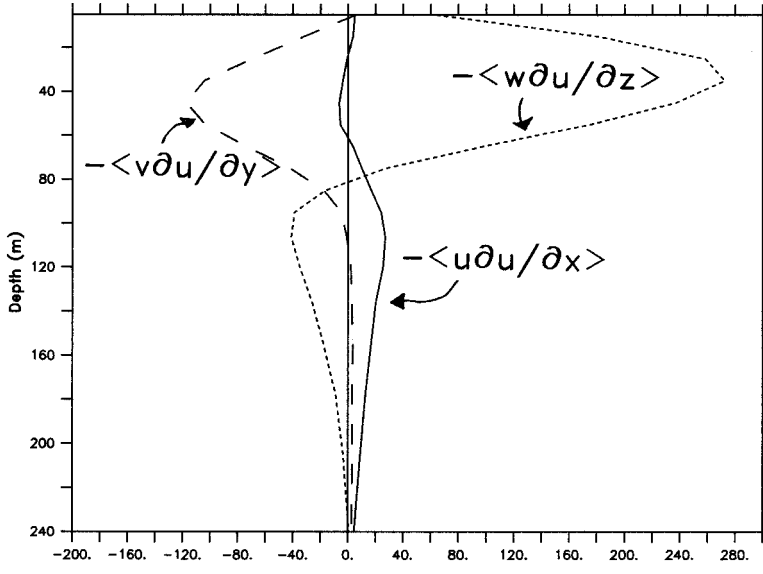

Figure 7. Vertical profiles of the three component terms of the total annual mean nonlinear zonal acceleration (cm/s/month), at (140W, 0N), as a function of depth.

40 m and the core of the EUC the picture is the same, but by 1S or 1N the advection, Coriolis and EDDY tendencies have all changed sign so that the primary eastward tendency is from the zonal pressure gradient tendency alone. The equatorial panel (Fig. 6e) shows the importance of nonlinearity above the EUC core very clearly.

Figure 7 shows vertical profiles of the three component terms of the nonlinear acceleration, at (140W, 0N). Above the EUC core zonal advection $-\langle u\partial u/\partial x\rangle$ is small, and vertical advection of eastward momentum $\langle w\partial u/\partial z\rangle$ from the EUC is only partially balanced by the near-surface Ekman-driven meridional advection $-\langle v\partial u/\partial y\rangle$. The near-surface eastward nonlinear advective tendency shown in Figure 6d is the result of this imbalance. Accurate estimation of each term is crucial if the nonlinear tendency is to be obtained. In and below the EUC core, meridional advection is small, and vertical advection $-\langle w\partial u/\partial z\rangle$ is roughly balanced by zonal advection $-\langle u\partial u/\partial x\rangle$; the residual is an $O(1)$ term that acts to decelerate the EUC. Note that these nonlinear tendencies are similar to those obtained by Wacongne, (1989: Fig. 8) in and above the EUC in the eastern Atlantic.

5. Vertically integrated zonal momentum balance

As noted in the Introduction, YM estimated the dynamical balances from time series of the TAO array. Without being able to estimate either the vertical or meridional advection, they concluded that, in the mean, the zonal momentum balance is primarily between zonal wind stress and depth-integrated zonal pressure gradient; i.e., a linear Sverdrup momentum balance on the equator. Their depth-integrated zonal advective term is relatively weak (5–15% of the wind stress term; see Table 1 from YM). The analysis in QW also suggests a

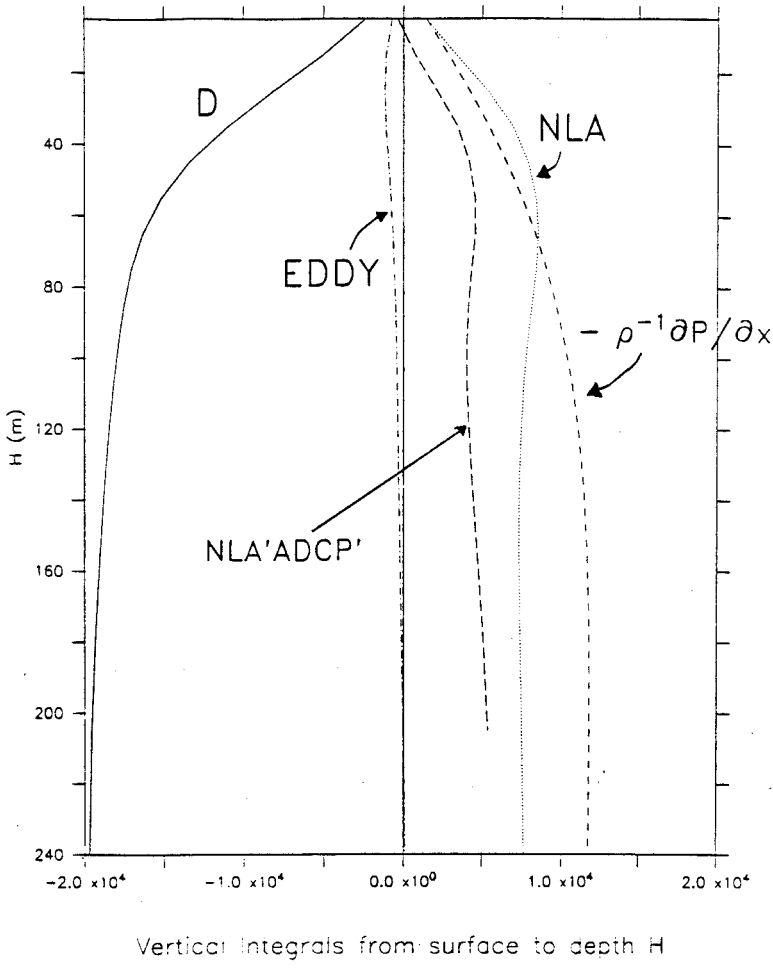

Figure 8. Vertically integrated (from the surface) annual mean zonal momentum terms ($cm^3/s/$ month), at (140W, 0N), as a function of depth. NLA = nonlinear advection of the mean zonal flow by the mean flow (see Eq. 5a in text), EDDY = eddy Reynolds stress divergence tendency (see Eq. 5b in text), $D = D_H + D_Z$ = mixing tendency (wind stress and friction; see Eqs. 6a and 6b in text). The vertically integrated 'ADCP-sampled' nonlinear advective term is labeled ADCP-NLA, and is discussed in Section 7. This is the nonlinear term estimated using observational constraints imposed by the TIWE field experiments: The ADCP-sampled velocities were obtained by using our model output u and v velocity fields, but u and v above 30 m were estimated by linear extrapolation using the 30–40 m shear. ADCP-sampled vertical velocity was computed by finite differencing the ADCP-sampled horizontal velocities on the coarse TIWE mooring grid. See text (Section 7) for discussion.

rough near-surface balance between the vertically integrated pressure gradient and the vertical stress divergence $\langle \partial \tau^x / \partial z \rangle$, with any imbalance resulting in a material acceleration (see Fig. 13 from QW where, above the core of the EUC, nonlinear terms account for less

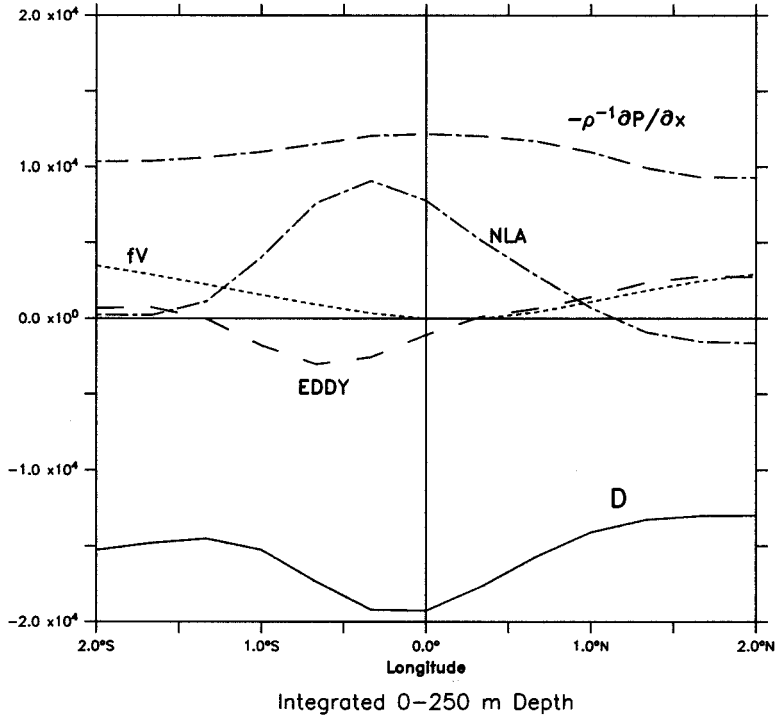

Figure 9. Vertically integrated (from the surface to 250 m depth) annual mean zonal momentum balance at 140W, between 2S to 2N. NLA = nonlinear advection of the mean zonal flow by the mean flow (see Eq. 5a in text), EDDY = eddy Reynolds stress divergence tendency (see Eq. 5b in text), $D = D_H + D_Z$ = mixing tendency (wind stress and friction; see Eqs. 6a and 6b in text). Units are $cm^3/s/month$. Extending the integration vertically to greater depth does not qualitatively change the result.

than 10% of the balance). JL arrived at a similar conclusion: in the vertical integral, the pressure gradient and the Coriolis force roughly balance the surface wind stress. Figure 8 shows the vertically integrated annual-averaged zonal momentum tendencies from our simulation, at 140W, and the equator, as a function of depth. The model results differ at order (1) from the observational estimates.

Figure 9 shows the integrals at 250 m (integration is from the surface to 250 m depth; extending the integration vertically to greater depth does not change the result) between 2S to 2N. Poleward of 1° the vertically integrated mixing tendency $\int D dz$ is dominated by the zonal wind stress at the surface, and is mostly balanced by the vertically integrated pressure gradient and Coriolis tendencies, i.e.,

$$\int_0^z \left(\frac{\partial P}{\partial x} + fV \right) dz \approx \langle \tau^x \rangle. \tag{8}$$

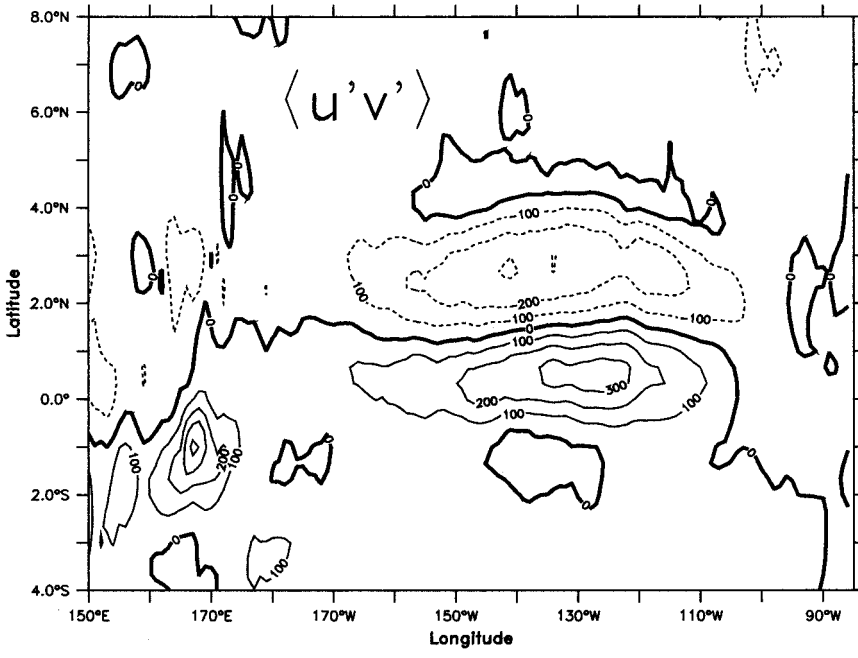

Figure 10. Annual mean surface Reynolds stress correlation $\langle u'v' \rangle$. Contour interval = 100 cm^2/s^2.

thus, off-equator the model balance is roughly "Sverdrup."

However, near the equator, the vertically integrated nonlinear terms play an order (1) role. Above the core of the EUC (see Fig. 9), the nonlinear terms are the same magnitude as the integrated pressure gradient tendency; integrated to 250 m, the nonlinear terms account for 30–40% of the wind stress term in the balance. In our model results, equatorward of 1°, the linear Sverdrup balance does not hold. In Section 7, we shall discuss a number of reasons why the reported observational results may underestimate near-surface nonlinearity.

6. Tropical instability waves

Early work in modeling the seasonal cycle of the tropical oceans (e.g., Philander *et al.,* 1986) advanced the notion that the effect of TIWs is similar to that of horizontal diffusion, and that numerical models with a resolution too coarse to resolve the TIWs can simulate their effect by using a larger horizontal eddy coefficient. The annual mean zonal momentum balances described above indicate that, at (140W, 0N), nonlinear effects due to TIWs are not a dominant term. However, they do contribute a zonal momentum tendency to accelerate the westward near-surface flow toward the west (Fig. 6d). In this sense, the TIWs are a 'negative viscosity' zonal momentum process over the upper 40 m and near the equator in this model geophysical system. How realistic does this result appear to be? Let

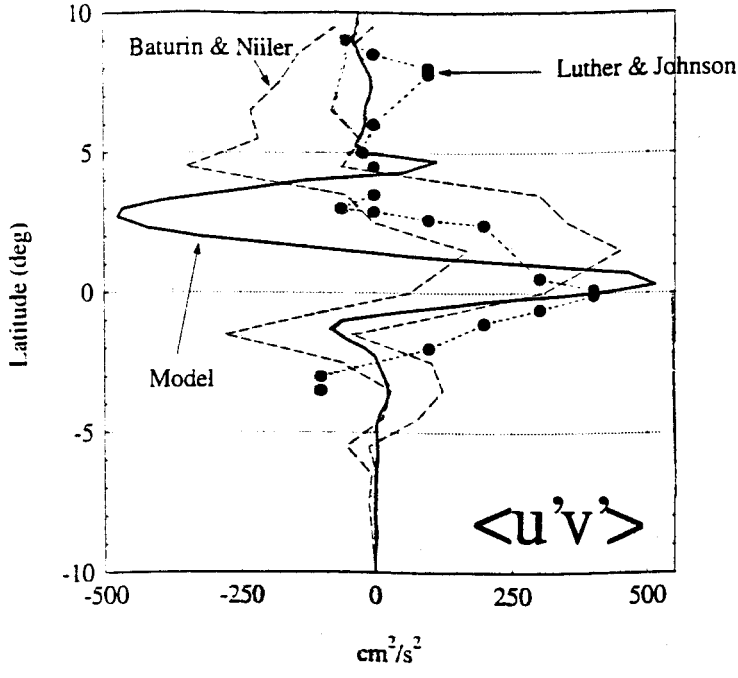

Figure 11. Comparison of estimated near-surface meridional structure of (a) $\langle u'u' \rangle$, (b) $\langle v'v' \rangle$ and (c) $\langle u'v' \rangle$ at 140W from the model (solid line) with observed correlations from Baturin and Niiler (1997; dashed lines) and Luther and Johnson (1990, solid circles). Units are cm^2/s^2. Baturin and Niiler analyzed over 1900 Lagrangian drifters in the equatorial Pacific from 1980 to 1994 and computed the averages during time periods when TIWs were active. Luther and Johnson estimated the correlations using ADCP velocities collected during the Hawaii-to-Tahiti Shuttle experiment in 1979–1980. For the Baturin and Niiler data, the envelope indicating $\pm$ one standard deviation are shown.

us consider how the model TIW zonal momentum flux terms compare with those reported from surface drifting buoys and from the Hawaii-Tahiti Shuttle ADCP data, which were collected between 150W and 158W.

A measure of the magnitude and location of the instability that produces TIW energy in the model is the structure of the annual mean of the Reynolds stress correlation $\langle u'v' \rangle$ (see, e.g., Luther and Johnson, 1990 and Baturin and Niiler, 1997). In Figure 10, we show the pattern of this field for our reference seasonal cycle numerical experiment. In this experiment there is an equatorial band of positive values with maximum amplitude of about 350 cm^2/s^2 and a negative band centered about 3N with maximum values of about -275 cm^2/s^2. Figure 11 shows a comparison of estimated near-surface meridional structure of $\langle u'u' \rangle$, $\langle v'v' \rangle$ and $\langle u'v' \rangle$ at 140W with similar correlations from Baturin and Niiler (1997) and Luther and Johnson (1990) somewhat farther west. Baturin and Niiler analyzed over 1900 Lagrangian drifters in the equatorial Pacific from 1980 to 1994 and computed

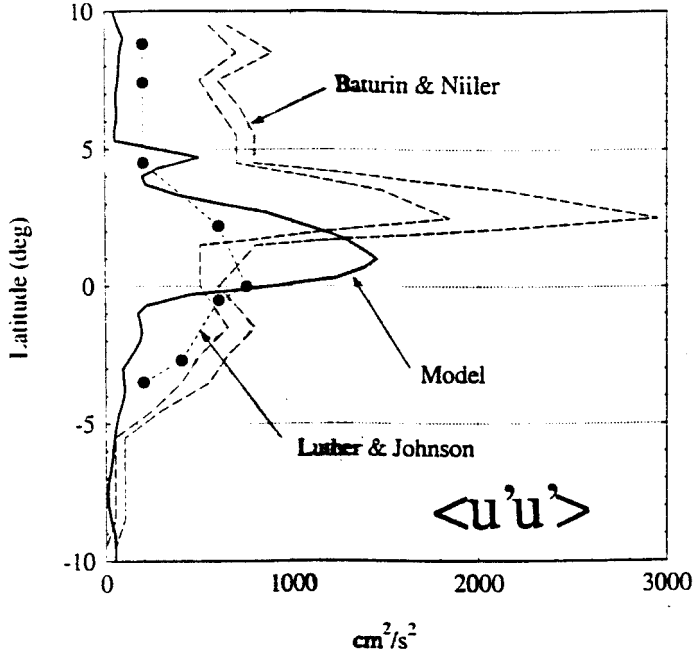

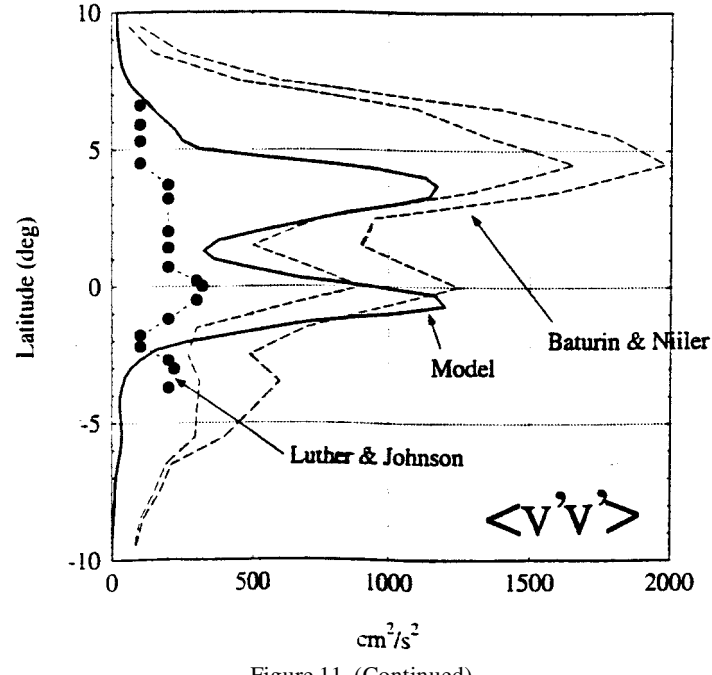

Figure 11. (Continued)

Table 1. Comparison between observational data and model prediction of near-surface $\langle u'u' \rangle$, $\langle v'v' \rangle$ and $\langle u'v' \rangle$ correlations at 140W near the equator. Brackets denote averaging during time periods when TIWs are active. Units are cm^2/s^2.

	Baturin & Niiler (1997)			Luther & Johnson	TAO	Model
	Min	Mean	Max	(1990)	data	prediction
$\langle u'u' \rangle$	1850	2400	2950	800	1209	1500
$\langle v'v' \rangle$	900	1100	1250	350	695	1200
$\langle u'v' \rangle$	170	300	450	420	245	500

the $\langle u'u' \rangle$, $\langle v'v' \rangle$ and $\langle u'v' \rangle$ correlations, averaged during time periods when TIWs are active. Near the equator, the peaks in our model correlations (averaged the same way) are similar to the Baturin and Niiler data (see Table 1) and the qualitative meridional structures have many similarities. However, the numerical model tends to compress the active region closer to the equator. A detailed comparison with Baturin and Niiler should be made with a model hindcast that includes El Nino, La Nina and "climatological" years. Luther and Johnson estimated the correlations using ADCP velocities collected during the Hawaii-to-Tahiti Shuttle experiment in 1979–1980. The ADCP correlations from Luther and Johnson and from the TAO buoy at 140W, also listed in Table 1, tend to be somewhat lower than both the Baturin and Niiler values and the correlations estimated with our model. This may reflect the ADCP under-sampling of the near-surface currents, where the TIWs are highly energetic in the numerical model (and also presumably in the ocean), or may also arise from the zonal dependence of these statistics or sampling issues arising from interannual variability.

Figure 12 shows $-U\partial\langle u'v' \rangle/\partial y$, the eddy-mean interaction term corresponding to the

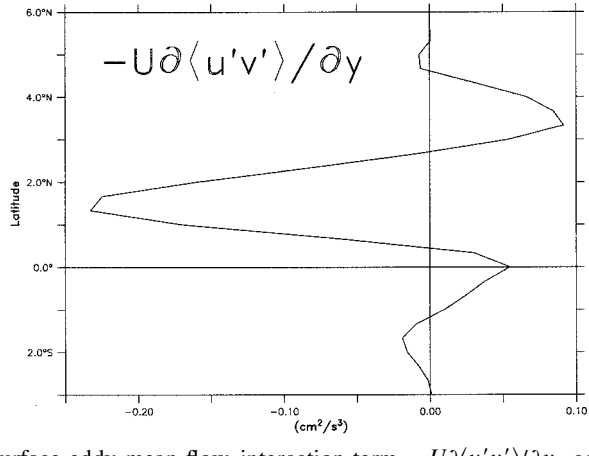

Figure 12. Near-surface eddy-mean flow interaction term $-U\partial\langle u'v' \rangle/\partial y$, corresponding to the work done on the mean flow in the energy equation by one component of the eddy Reynolds stresses. Units are cm^2/s^3.

work done on the near-surface mean flow in the energy equation by one component of the eddy Reynolds stresses (e.g., Harrison and Robinson, 1978). Figure 12 indicates how the TIW meridional transport of zonal momentum does work on the zonal currents: Some of the momentum extracted from the mean flow by the waves just north of the equator (0.5–2N; presumably the source region for the instability) is returned to the mean flow at and just south of the equator (1S–0.5N). This topic will be revisited in our companion paper (Harrison *et al.,* 2001), where we show that the seasonal variations in TIW zonal momentum tendency play an important role in the seasonal reversal of the near surface flow.

7. Discussion

The results of a climatologically forced primitive equation ocean circulation model simulation of the seasonal cycle of upper ocean currents are in good agreement with observations at (140W, 0N). We have used this simulation to study the balances that control the model zonal flow. The numerical model allows us to evaluate the terms in the zonal momentum equation on a model grid with relatively high resolution. The model annual mean values reported here are obtained from a 'seasonal cycle' numerical experiment in which the near-surface cycle repeats almost exactly in and above the thermocline. The annual means are quasi-stationary.

The annual mean momentum balances at (140W, 0N) are fully three-dimensional. Dynamical balances are very different within the upper 40 m, and over the region just above and below the core of the EUC. The mean zonal pressure gradient tendency ($-\rho^{-1}\partial P/\partial x$) is eastward from the surface and down throughout the EUC (the EUC is still accelerating at this longitude in this experiment). The net nonlinear advective tendency (NLA) from the annual mean flow is eastward above the core of the EUC and between 2S and 4N is dominated by vertical advection. The wind stress and mixing tendencies are westward, as is the eddy zonal momentum tendency (EDDY), which is defined at this stage to include the nonlinear effects of the seasonal flow and the tropical instability waves. The primary balance above the core of the EUC is between wind stress (westward) and a combination of NLA and $-\rho^{-1}\partial P/\partial x$ (eastward). EDDY is a significant but not dominant term, being one-fifth to one-third the amplitude of the largest equatorial tendencies; its tendency is to retard the EUC above the core and within 1S and 1N. Farther out on the northern flank of the EUC the eddies tend to accelerate the EUC and to decelerate the SEC flow. Below the core of the EUC there is considerable meridional structure in the tendencies. The equatorial balances are not typical of the balances at 0.67° latitude (two grid points poleward); there $-\rho^{-1}\partial P/\partial x$ remains eastward and wind stress westward, but NLA is now westward and fV can be order one in the balance. Equatorward of 1°, the vertically integrated zonal momentum balances (Fig. 9) indicate that an above-thermocline linear equatorial Sverdrup balance does not hold in the annual mean.

The individual zonal mean advection components show meridionally asymmetric cellular structures; none of the terms is symmetric about the equator. The nonlinear term

$-U\partial U/\partial x$ is relatively unimportant above the core of the EUC. Above the core of the EUC, and equatorward of 1°, $-W\partial u/\partial z$ dominates, however $-V\partial U/\partial y$ is significant, particularly in the northern hemisphere. Poleward of 1°, $-V\partial U/\partial y$ dominates. Below the EUC, meridional advection is small, and vertical advection is balanced by zonal advection; the residual acts to decelerate the EUC downstream.

There are a number of factors that may contribute to the difference between the zonal momentum balances inferred from the numerical model results and those presented by YM, QW, and LJ. They are: (1) inability of the subsurface acoustic Doppler current meter profilers (ADCP) and the ship-borne ADCP to adequately resolve the currents shallower than 30 m (where the model says observations are critical), (2) coarse horizontal resolution of measurements, which leads to inaccurate estimates for vertical velocity (QW), (3) inability to compute $\partial/\partial y$ and w at all (YM), (4) the fact that there is lots of variability on subseasonal and interannual time scales that affects estimates of long-time means from short-time series (LJ and QW) and from only monthly samples (LJ). In particular, the amplitude of TIW energy and Kelvin pulse energy can be very different from year to year, and El Nino, La Nina and 'normal' years also have substantially different large-scale flow structures. Finally, (5), as we noted previously, there are zonal gradients in the momentum balances which can introduce differences of detail in our comparison with JL, where the data were collected west of 140W.

To investigate the consequences of the vertical extrapolation done in each of the observational studies and of the horizontal differencing done in QW, we sampled our model u and v velocity fields as if they were ADCP data and then followed the data processing done in QW. Thus, u and v above 30 m were estimated by linear extrapolation based on the 30–40 m shear; then horizontal derivatives and the resulting estimate for w were computed on the relatively coarse TIWE mooring grid using the QW differencing and integration algorithm, (discussed in their Appendix). Figure 13 compares these 'ADCP-sampled' and full-vertical resolution model annual mean velocity profiles at (140W, 0N). The ADCP-sampled zonal velocity near the surface is lower by a factor of two. The strong shear in the near-surface meridional velocity is not well represented, and the ADCP-sampled v is of opposite sign near the surface. The computed mean ADCP-sampled vertical velocity above 100 m is underestimated by nearly a factor of two.

How do these differences affect the estimated zonal momentum equation balances? The ADCP-sampled nonlinear contribution to the zonal momentum balance is greatly reduced for depths less than 80 m (above the EUC). The vertically integrated ADCP-sampled nonlinear term is plotted on Figure 8; above the EUC the ADCP-sampled nonlinear term contribution to the integrated momentum balance is reduced by almost a factor of two relative to the full model result. Examination of the advective terms shows that this is primarily due to underestimation of the near-surface vertical advection of momentum ($-W\partial U/\partial z$), but there are consequences from errors in the meridional advection term ($-V\partial U/\partial y$). However, within the thermocline (80–150 m) the pattern of NLA from the model and from JL is similar. But JL have smaller equatorial $W\partial U/\partial z$ because their

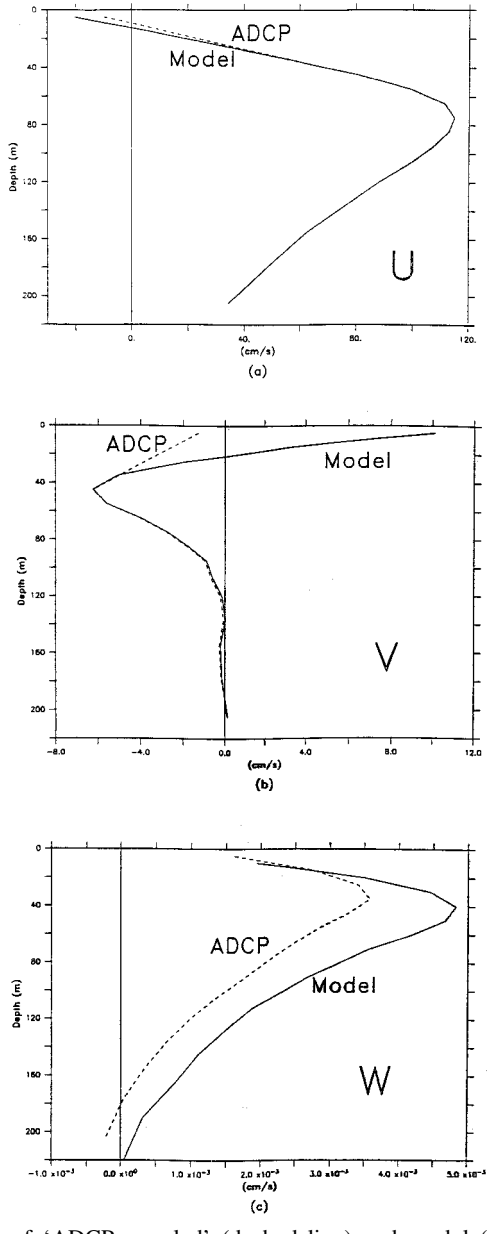

Figure 13. Comparison of 'ADCP-sampled' (dashed line) and model (solid line) annual mean velocity profiles at (140W, 0N). (a) zonal velocity (U; cm/s; positive eastward), (b) meridional velocity (V; cm/s; positive northward), (c) vertical velocity (W; cm/s; positive vertically upward). The ADCP-sampled velocities were obtained by using our model output u and v velocity fields, but u and v above 30 m were estimated by linear extrapolation using the 30–40 m shear. ADCP-sampled vertical velocity was computed by finite differencing the ADCP-sampled horizontal velocities on the coarse TIWE mooring grid. The ADCP-sampled zonal velocity near the surface is lower by a factor of two. The strong shear in the near-surface meridional velocity is not well-represented, and the ADCP-sampled v is of opposite sign near the surface. The computed mean ADCP-sampled vertical velocity above 100 m is underestimated by a factor of two.

equatorial W is smaller (see their Fig. 9). Despite the smaller vertical advection tendency, JL found that NLA term was part of the basic balance in the EUC and tended to decelerate the EUC, as is found in the model balances.

This simple exploration does not establish that the model zonal momentum balances are correct or prove that the vertically integrated observational balances are incorrect. However, it raises the strong possibility that experimental constraints associated with the observations recently analyzed in the equatorial Pacific Ocean may limit their ability to be definitive about near-surface current profiles and zonal momentum balances. It suggests that it is particularly unwise to attempt to make zonal momentum balance estimates simply from widely zonally spaced moorings (YM). The complex meridional and vertical structures of the individual advective terms and the fact that meridional and vertical advection are each order (1) but of opposite sign means that these terms must be estimated very accurately if the importance of nonlinearity near the surface is to be evaluated.

Because this experiment was forced with climatological wind stresses, we cannot estimate the implications of the observations having been taken over different time intervals in a strongly variable ocean environment or of having been relatively infrequently sampled. The model would have to be run in hindcast mode, over the time period spanning all of the observations in order to make such estimates.

The model annual mean zonal momentum equation balances show very strong spatial structure in depth and with latitude in and near the equatorial Pacific waveguide. Within the latitude range of 4S to 4N and the depth range of the surface to 250 m we find that every term in the model momentum equation is $O(1)$ somewhere. The crucial next observational step, to begin to evaluate the extent to which the model flows and balances are like those of the ocean, is to resolve the currents of the upper 40 m of the water column. The information can be collected at relatively low cost (certainly at low cost compared with dynamical balance arrays) with existing technology.

Acknowledgments. The authors thank George Philander and Ron Pacanowski for developing and sharing this version of the Bryan-Cox-Semtner ocean GCM, which is now incorporated within the Modular Ocean Model framework (Pacanowski, 1995). Gabe Vecchi and Ed Sarachik offered valuable discussion and editorial help. Two anonymous reviewers contributed substantially to the details of the final form of this paper. Ed Sarachik presented an early version of these results at an Equatorial Theory Panel meeting in 1991. The PMEL TMAP group offered valuable assistance. Many of the numerical experiments were done at the Alaska Region Supercomputer Center. The authors were supported by NOAA (OAR HQ, Office of Global Programs and PMEL) and by NASA [Order # W19,533 (Physical Oceanography)]. This is PMEL contribution 2196 and JISAO publication #802.

REFERENCES

Baturin, N. G. and P. P. Niiler. 1997. Effects of instability waves in the mixed layer of the equatorial Pacific. J. Geophys. Res., *102* (C13), 27771–27793.

Harrison, D. E. 1989. On climatological monthly mean wind stress and wind stress curl fields over the world ocean. J. Climate, *2,* 57–70.

—— 1991. Equatorial SST sensitivity to net surface heat flux: Some ocean circulation model results. J. Climate, *4,* 539–549.

—— 1996. Vertical velocity variability in the central tropical Pacific—a circulation model perspective for JGOFS. Deep-Sea Res. II, *43,* 687–705.

Harrison, D. E., W. Kessler and B. Giese. 1989. Hindcasts of the 1982–83 El Nino: Thermal and dynamic height variability along the ship of opportunity XBT tracks. J. Phys. Oceanogr., *19,* 397–418.

Harrison, D. E., R. D. Romea and G. A. Vecchi. 2001. Central equatorial Pacific zonal currents. II: The seasonal cycle and the boreal spring surface eastward surge. J. Mar. Res., *59,* 921–948 (this issue).

Harrison, D. E. and A. R. Robinson. 1978. Energy analysis of open regions of turbulent flows—mean eddy energetics and a numerical ocean circulation experiment. Dyn. Atmos. Oceans, *2,* 185–211.

Johnson, E. S. and D. S. Luther. 1994. Mean zonal momentum balance in the upper and central equatorial Pacific Ocean. J. Geophys. Res., *99* (C4), 7689–7705.

Large, W. G. and S. Pond. 1981. Open ocean momentum flux measurements in moderate to strong winds. J. Phys. Oceanogr., *11,* 324–336.

Levitus, S. 1982. Climatological Atlas of the World Ocean, NOAA Prof. Paper 13, U.S. Govt. Printing Office, Washington DC, 173 pp.

Luther, D. S. and E. S. Johnson. 1990. Eddy energetics in the upper equatorial Pacific during the Hawaii-to-Tahiti Shuttle experiment. J. Phys. Oceanogr., *20,* 913–944.

McPhaden, M. J. and S. P. Hayes. 1990. Variability in the eastern equatorial Pacific during 1986–88. J. Geophys. Res., *95,* 13,195–13,208.

Pacanowski, R. C. 1995. MOM 2 Documentation, User's Guide and Reference Manual, Version 1.0, Sept 30, 1995, GFDL Ocean Technical Report #3.

Pacanowski, R. C. and S. G. H. Philander. 1981. Parameterization of vertical mixing in numerical models of tropical oceans. J. Phys. Oceanogr., *11,* 1443–1451.

Philander, S. G. H., W. J. Hurlin and R. C. Pacanowski. 1986. Properties of long equatorial waves in models of the seasonal cycle in the tropical Atlantic and Pacific oceans. J. Geophys. Res., *91,* 14207–14211.

Philander, S. G. H., W. J. Hurlin and A. D. Seigel. 1987. Simulation of the seasonal cycle of the tropical Pacific Ocean. J. Phys. Oceanogr., *17,* 1986–2002.

Philander, S. G. H. and R. C. Pacanowski. 1981. Response of equatorial oceans to periodic forcing. J. Geophys. Res., *86,* 1903–1916.

Philander, S. G. H. and A. D. Seigel. 1985. Simulation of El Nino of 1982–83, *in* Coupled Ocean Atmosphere Models, J. Nihoul, ed., Elsevier, 517–541.

Qiao, L. and R. H. Weisberg. 1997. The zonal momentum balance of the equatorial undercurrent in the central Pacific. J. Phys. Oceanogr., *27,* 1094–1119.

Stockdale, T. N., A. J. Busalacchi, D. E. Harrison and R. Seager. 1998. Ocean modeling for ENSO. J. Geophys. Res., *103* (C7), 14,325–14,356.

Wacongne, S. 1989. Dynamical regimes of a fully nonlinear stratified model of the Atlantic Equatorial Undercurrent. J. Geophys. Res., *94,* 4801–4815.

—— 1990. On the difference in strength between Atlantic and Pacific undercurrents. J. Phys. Oceanogr., *20,* 792–799.

Woodruff, S. D., R. J. Slutz, R. L. Jenne and P. M. Steurer. 1987. A comprehensive ocean-atmosphere data set. Bull. Amer. Meteor. Soc., *68,* 1239–1250.

Yu, X. and M. J. McPhaden. 1999a. Dynamical analysis of seasonal and interannual variability in the equatorial Pacific. J. Phys. Oceanogr., *29,* 2350–2369.

—— 1999b. Seasonal variability in the equatorial Pacific. J. Phys. Oceanogr., *29,* 925–947.

Received: *27 January, 2001;* revised: *6 August, 2001.*